3D effects on flutter prediction in aeronautic compressor

P. DUQUESNE[a], B. MAHIEUX[b], S. AUBERT[a], P. FERRAND[a]

a. Univ Lyon, Ecole Centrale de Lyon, INSA Lyon, Université Claude Bernard Lyon I, CNRS, LMFA, UMR 5509, 36 Avenue Guy de Collongue, F-69134, ÉCULLY, France. pierre.duquesne@ec-lyon.fr
b. Safran Aircraft Engines, Moissy-Cramayel, France. bruno.mahieux@safrangroup.com

Résumé :

Le flottement correspond à un chargement aérodynamique qui amplifie les modes propres de la structure. Cette interaction entre le fluide et la structure peut mener à la destruction des aubages du compresseur. Lors des premières phases de conception d'un compresseur, le déclenchement du flottement est estimé dans un plan 2D (coupe aube à aube, proche du carter). Sur des géométries modernes, plusieurs études montrent une différence entre cette prédiction et les essais expérimentaux. Dans cet article, des simulations numériques 2D et 3D ont été effectuées sur la roue d'une géométrie moderne de compresseur axial pour évaluer les limites de l'approche 2D.
Le logiciel elsA a été utilisé pour obtenir le champ stationnaire à partir d'une simulation RANS (Reynolds-Averaged Navier-Stokes) avec un modèle de turbulence k-ω. Le mouvement imposé à l'aube correspond au premier mode de torsion avec deux diamètres nodaux. Par la suite, les fluctuations de l'écoulement ont été déterminées en utilisant le solveur RANS linearisé en temps Turb'lin.
Selon les conditions d'opération, les ondes de pression régressives provenant du bord de fuite peuvent remonter l'écoulement jusqu'à l'onde de choc. En se rapprochant de l'onde de choc, l'amplitude des ondes de pression augmente et induit d'importantes fluctuations de pression. Dans un calcul 3D, les ondes de pression peuvent s'échapper dans la direction radiale. Cette déviation radiale ne peut par contre pas être capturée avec un calcul 2D et cela modifie l'échange de travail.

Abstract :

The flutter corresponds to an aerodynamic loading which amplifies the natural vibration of the structure. This fluid-structure interaction can lead to the failure of compressor blades. In the design stage, the detection of flutter is estimated in a 2D radial plan (a blade to blade cut, near the shroud). The studies on modern designs point to some disparity between these predictions and experimental test. In this paper, 3D and 2D simulations have been conducted on the rotor of a modern design of high pressure axial compressor to investigate the limitations of the 2D approach.
To solve the steady flow, the Reynolds-Averaged Navier-Stokes (RANS) simulations with k-ω turbulence model has been performed with elsA solver. The blade motion corresponding to the first torsion mode at two nodal diameters has been imposed on the blade. Then, the flow fluctuations have been determined by the time-linearized RANS solver Turb'lin.
Depending on the operating condition, regressive pressure waves from the trailing edge can travel up to the shock wave. Approaching the shock wave, pressure wave amplitudes increase and induce important

pressure fluctuations. In the 3D calculation pressure waves can escape in radial direction. The pressure wave radial deviation cannot be captured with a 2D calculation and has an impact on the work exchange.

Mots clefs : flutter, compressor, L-URANS

1 Introduction

The flutter is a fluid-structure interaction corresponding to an aerodynamic loading of the structure which amplifies the natural vibration of the structure. This fluid-structure interaction can lead to the failure of compressor blades, and the associated catastrophic consequences for the entire turboreactor.
In the early design stage, the detection of flutter is estimated on a 2D radial cut (blade to blade channel, near the shroud) with numerical simulations or with some empirical design criteria as the Torsion to Bending Coupling [1]. Industrial tests on modern designs point to the failure of these methodologies. Numerous origins can explain the non-ability to accurately predict the flutter triggering. In the case of numerical prediction, the turbulence model [2], the acoustic waves or the 2D restriction are only some examples. For axial compressors, due to higher computational cost, the 3D calculations seem difficult to perform in the design stages for all operating points (and for multiple mechanical modes). For fans, 3D flutter calculations have been achieved in recent years and point to the predominance of the upper part of the blade in the work exchange [1,3]. In [4], a fan blade is analysed based on 3D simulations, in this case the exchanged work is huge at the shock wave. Depending on the height, the exchange can be destabilising or not. In the same paper, authors try to track the source of the instability in the radial direction but the flutter mechanism keeps unclear.
This paper aims to discuss the 2D approach in the flutter triggering prediction. A high pressure axial compressor test case is analysed at two operating points using linearised RANS simulations. Both operating points are at partial speed and present large supersonic zones. The first torsion mechanical mode with two nodal diameters has been imposed. 2D and 3D simulations have been performed. These cases are selected to be representative to a situation where the 2D approach gives a good approximation of 3D results in one case and the opposite in the other case.

2 Numerical methods

2.1 Steady solver

ONERA elsA CFD software is used for the 3D and 2D steady state calculations. A Jameson convective flux [5] with second and fourth order dissipations is used. The selected turbulence model is the k-ω turbulence model of Kok [6]. The source term of the turbulent transport equations is computed from vorticity rather than from the strains tensor to avoid turbulent overproduction near the leading edge and across the shock wave.
Following the industrial practice, the 3D-structured mesh of the isolated rotor consists of around 1 600 000 points. The final 2D mesh consists of around 20 000 points. The grid convergence has been checked with a 2D mesh with 80 000 points.
The 3D calculation is performed first. The 2D geometry and the corresponding mesh are extracted from the 3D solution. The blade to blade cut is obtained for a constant height near 80%. This choice has been motivated by the good practices in flutter prediction and because the majority of the amount of work is

exchanged at the upper part of the blade. The selected height is not at the shroud to avoid local phenomena as the blade tip vortex. In consequence of the constant height the cut is curved and needs to be flattened.
The radial velocity component is generally small in axial turbomachinery application. In a 2D calculation, the radial velocity component is assumed null. To conserve the same level of energy, the 3D radial component is distributed between the two other components for the 2D simulation. The velocity redistribution preserves the flow angle between the axial and circumferential components and the total velocity vector norm. The total pressure, the total energy and the turbulence variables used as 2D boundary conditions are extracted from the 3D result. Because 3D losses cannot be represented in 2D, the inlet azimuthal velocity and the outlet static pressure are adjusted to conserve the position and the pattern of shock waves between the 2D and the 3D solutions at the same height.

2.2 Time-linearised URANS solver

The Linearised RANS (LRANS) solver Turb'Lin is used to compute the harmonic flow around the steady state. This solver has been previously validated on transonic separated flows [7,8]. The solution is obtained in the frequency domain by solving the linear system. Spatial discretisation relies on Jameson centred scheme with a linearised pressure sensor [5]. The frozen turbulence assumption is used in this study. The turbulence variables are kept constant at their values estimated by the RANS solver. This assumption means that the characteristic time of the turbulence evolution is very slow comparatively to the blade vibration characteristic time.

2.3 Aeroelasticity

The complex amplitudes of displacement $\widetilde{\delta \mathbf{x}}$ and velocity $\widetilde{\mathbf{V}}$ are imposed at each node of the blade mesh to model the blades oscillation.

The interblade phase angle (IBPA) σ is modelled through quasi-periodic boundary conditions in azimuthal direction

$$\widetilde{\boldsymbol{q}}(\boldsymbol{x_b} + \boldsymbol{g}) = \widetilde{\boldsymbol{q}}(\boldsymbol{x_b}) e^{\boldsymbol{j\sigma}} \tag{1}$$

where $\widetilde{q}$ is the complex amplitude of conservative variable fluctuations, x_b a node of the domain boundary and g the interblade pitch.

The local work $\mathcal{W}$ extracted by the flow from the structure is written according to the convention of Verdon [9].

$$\mathcal{W} = \int_0^T \left[-\widetilde{Ps}(\mathbf{x}, t) * \widetilde{\mathbf{S}}(\mathbf{x}, t) \right]^* \cdot \widetilde{\mathbf{V}}(\mathbf{x}, t) \mathrm{d}t \tag{2}$$

where $\widetilde{Ps}$ is the instantaneous static pressure, $\widetilde{\mathbf{S}}$ the vector associated with the instantaneous surface, oriented towards the structure.
Negative local work ($\mathcal{W}$< 0) denotes an exchange from the fluid towards the structure, a flutter case. In contrary positive local work denotes a stable configuration. The total work is the sum of the local work around the entire blade (or the entire profile in 2D) and allows to determine the blade stability.
The equation 3 can be decomposed with the introduction of the average part (superscript ^{0} before the quantity) and the fluctuating part (superscript ^{1}, as for Turb'lin calculations only the first harmonic is considered). With this decomposition two terms emerge for the flutter prediction. The first term is

associated with the effect of the average pressure field :

$$\mathcal{W}_s = -T\,{}^0Ps\,{}^1\widetilde{\mathbf{S}}^*.{}^1\widetilde{\mathbf{V}} \tag{3}$$

And the second part is associated with the pressure fluctuation field :

$$\mathcal{W}_u = -T\,{}^1Ps\,{}^0\widetilde{\mathbf{S}}^*.{}^1\widetilde{\mathbf{V}} \tag{4}$$

$\mathcal{W}_s$ can be directly computed from the steady pressure field and the blade motion but $\mathcal{W}_u$ needs the pressure fluctuation calculation.

3 Studied configuration

The high pressure compressor geometry has been designed by Safran Aircraft Engines to be representative of the state of art. Due to confidentiality concerns, all the figures have a modified aspect ratio and shape.

3.1 Mode shape

The mode shape is a result of the mechanical finite element analysis (FEA) software SAMCEF. The first torsion mode is imposed at each node of the blade mesh. As presented in fig. 1 with the displacement modulus, the mode is not a pure torsion. The name is selected from the comparison with other modes predicted by the FEA software. As can be noticed, the motion of the blade to blade cut at 80% heights include a bending contribution. To obtain the torsion mode for the 2D calculation, the mechanical mesh is projected on the aerodynamics mesh. The correspondence of the blade motion between the 3D motion and the 2D projected motion at the same height has been checked.

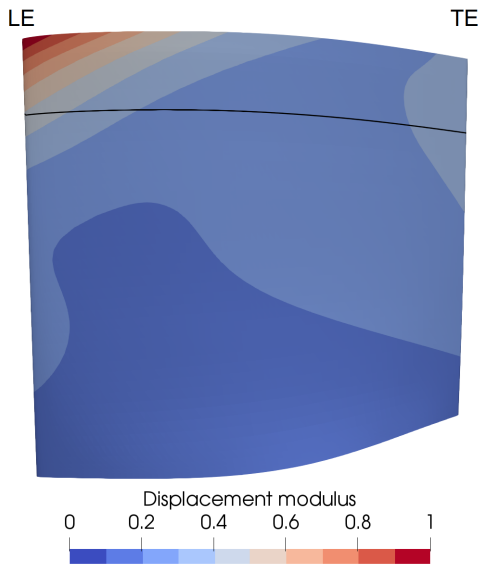

FIGURE 1 – Displacement modulus for the first torsion mode on the suction side. Black line represents the extraction at 80% blade height. LE : leading edge, TE : Trailing edge. 3D-blade shape is strongly deformed for industrial property concern.

It is assumed that all rotor blades have the same mode shape and the same frequency. Two adjacent blades can present a phase shift called interblade phase angle. In turbomachinery application, due to the cylindrical aspect of the geometry, the number of interblade phase angles is finite and can be represented by the nodal diameter. The nodal diameter (ND), the interblade phase angle (σ) and the total number of blades (N) are linked by :

$$\sigma = 2\pi ND/N \tag{5}$$

Only the case at $2ND$ is presented in this paper.

3.2 Global steady flow pattern

Fig. 2 presents the map of the Mach number on a blade to blade cut at 80% height from the 3D calculation, the line at Mach number equal to 1 is presented in black. The two operating points selected are presented in fig. 2, respectively OPA and OPB at left and right .

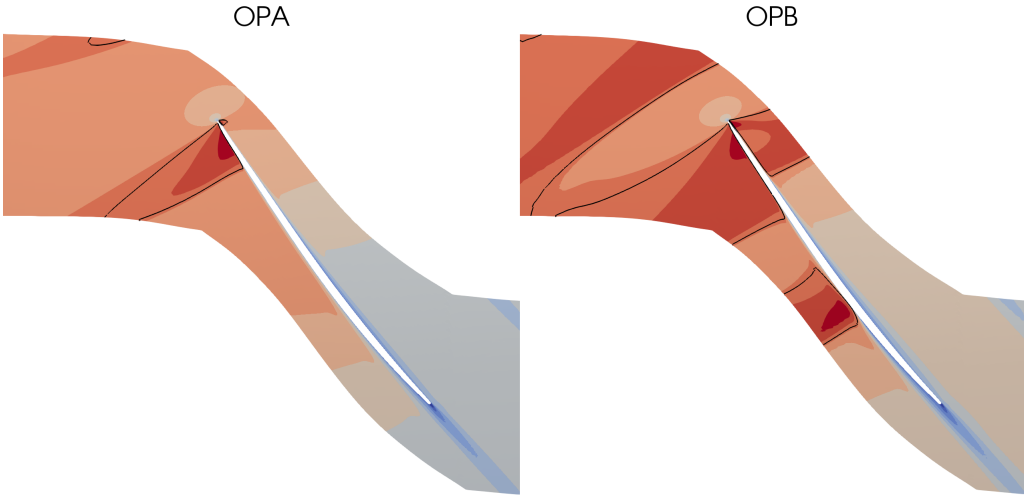

FIGURE 2 – Mach number field from low (blue) to high (red) values for OPA (at left) and OPB (at right). Isoline at Ma=1 is in black.

OPA is at partial speed (90 Nn) and the inlet axial velocity is subsonic. A large supersonic zone is present on the suction side near the leading edge. In the radial direction, the shock wave extends from the half of the blade height to the shroud. OPB is also at partial speed but higher than OPA (98 Nn). The inlet axial velocity is also subsonic. Like OPA, a large supersonic zone is present on the suction side near the leading edge. This supersonic zone is larger than for OPA and extends up to the front of the adjacent blade. For OPB, in addition a second supersonic zone appears downstream. The shock wave extends from the suction side to the pressure side and chokes the interblade channel at 80% height. The radial extension of these supersonic zones are comparable with the one at OPA. The radial extension of the downstream traversing shock wave is slightly larger than the upstream one. A small zone of flow separation is present on the suction side near the trailing edge.

In a 2D calculation a choice has to be made : conserve the shock wave position or conserve the level of losses. The goal of this calculation is not to predict the compressor performance but the flutter triggering. In this context the position of the shock wave is a predominant effect and the position needs to be conserved. As presented with the isentropic Mach number along the blade in fig. 3, the boundary condition of the 2D calculation has been adjusted to obtain the same shock wave position for OPA and

OPB. In consequence losses at the trailing edge are different between 2D and 3D calculation.

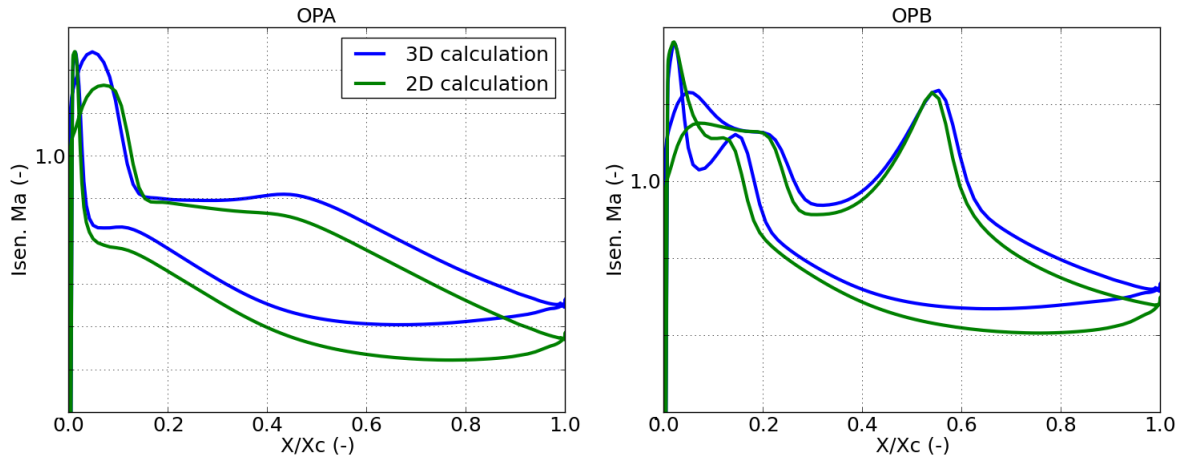

FIGURE 3 – Isentropic Mach number around the profile for OPA (at left) and OPB (at right). The 3D calculation is in blue and the 2D calculation is in green.

4 Analysis

4.1 Global flutter prediction

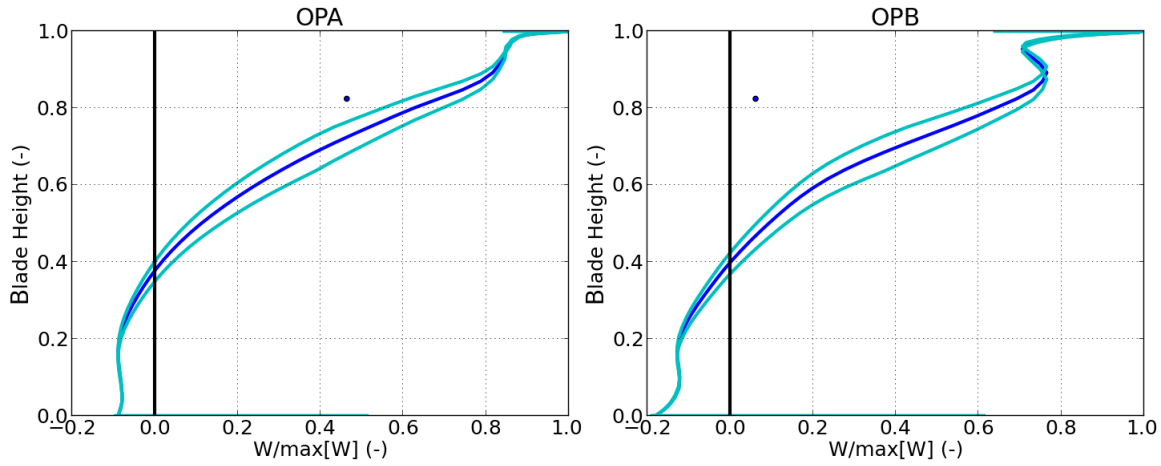

FIGURE 4 – Normalised work exchange along the blade height for OPA (at left) and OPB (at right). Dark blue lines represent the 3D result, light blue lines represent the 2D/3D position uncertainty and the blue dots represent the 2D result.

The sum of the work around the entire blade for the 3D calculation or the sum around the profile for the 2D calculation allow the determination of the blade global flutter stability. The direct comparison of the two values has no sense, only their sign can be directly interpreted. In all presented cases (OPA and OPB and with 2D and 3D calculations) the sum of the work is positive and consequently the cases are interpreted as stable. The dark blue line in fig. 4 presents the evolution of the sum of the total work exchanged around the profile along the radial direction extracted from the 3D results. For both OP, the

cut at 80% blade height is representative of the global stability : high enough to represent a dominant zone of the work exchange but not too much to be contaminated by the local effect near the shroud. The result of the 2D calculation is represented by a blue point in fig. 4. For OPA, the sums of the work at 80% have a similar value between the 2D and the 3D results (the difference is around 30%). For OPB, the difference between both calculations has more than 1 order of magnitude.
The work exchange induces by the steady pressure field ($\mathcal{W}_s$) is similar for the 2D and 3D results for OPA and OPB. These results support previous conclusions about the similarity of the steady field between 2D and 3D calculation (as shown in fig. 3 with the isentropic Mach number) and the projection of the blade motion in a 2D plane. The large difference in prediction for OPB thus cannot be explained by the work exchange from the steady field. In the following, discussion based on the analysis of the pressure fluctuating field presents which phenomena can explain the bad prediction with a 2D calculation for OPB.

4.2 Work exchange local analysis

In this section, the pressure fluctuations are analysed. The first subsection is about OPA and presents a case where the 2D results are representative of the 3D prediction. The second subsection is dedicated to OPB and explains the difference that conducts to the large disparity between 2D and 3D results.

4.2.1 OPA : Good 2D/3D similarity

For OPA, the global pattern of the pressure fluctuation is similar in 2D and 3D. In both cases, pressure fluctuation modulus is larger in the upstream part of the blade (see fig. 5). The planar regressive pressure waves emitted in the neighbourhood of the trailing edge (see fig. 6) are amplified at the shock wave on the suction side and by the small supersonic pocket at the leading edge on the pressure side (see fig. 5). In the 3D result the spot where the regressive waves are emitted is more downstream and the interaction with the supersonic zone induces more intense pressure waves than for the 2D case. These can certainly be explained by the effect of other pressure waves coming from different heights of the blade. The global pressure fluctuations similarity between the 2D and 3D results at the same height indicates that the total work exchange value is not induced by some compensatory effect. In this case, the flutter triggering prediction using only a blade to blade cut seems reasonable.

4.2.2 OPB : Bad 2D/3D similarity

As shown in fig. 7, for OPB, zones of high pressure fluctuations are located at both shock waves in particular the downstream one. It is classical as motion of a shock wave which chokes the interblade channel induces large pressure fluctuations. Results of the 2D and 3D calculations are close. The 3D calculation induces stronger pressure fluctuations but the difference cannot explain the large disparity in the total work exchange noticed previously.

The pressure fluctuation phase field for OPB is presented in fig. 8. Some disparity is clear between 2D and 3D cases. On the pressure side, phase pattern for the 3D case indicates a source at the last third of the chord which induces regressive pressure waves up to the shock wave and progressive pressure waves up to the trailing edge. The phase field for the 2D case presents a more complex wave propagation. Regressive pressure waves seem to be emitted at the trailing edge but do not reach the shock wave. The

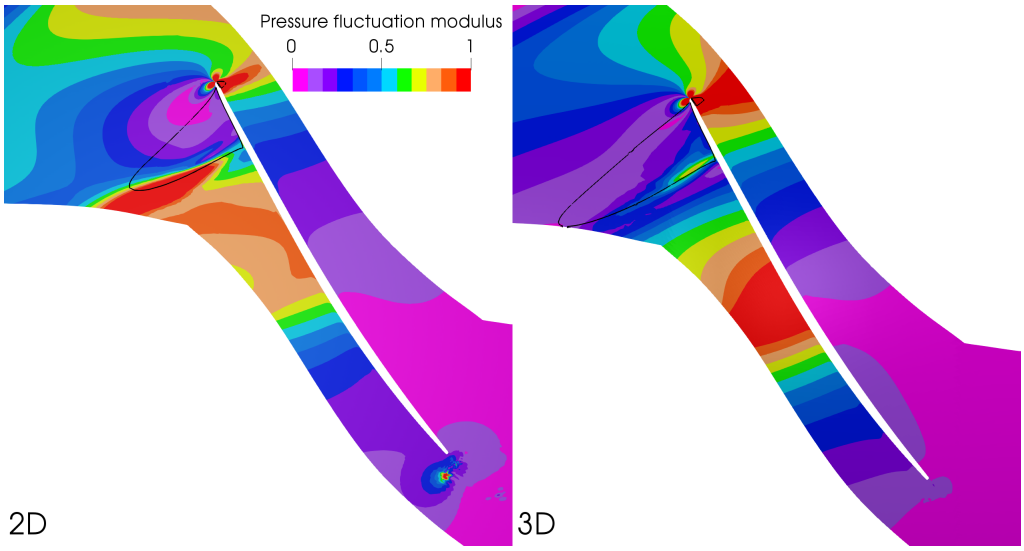

FIGURE 5 – Normalised pressure fluctuation modulus for OPA from the 2D calculation (at left) and the extraction at 80% blade height from the 3D calculation (at right), the line at Mach number equal to 1 is drawn in black.

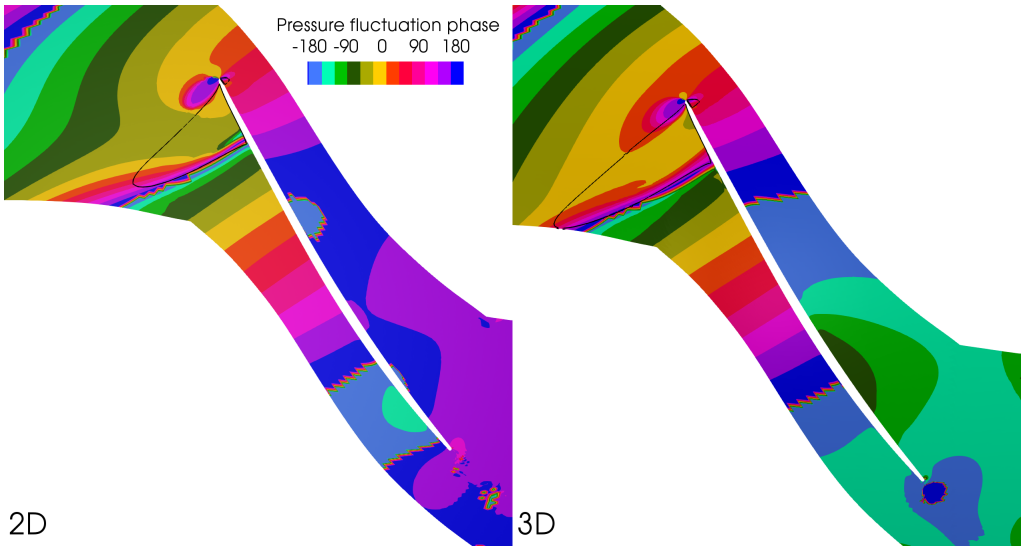

FIGURE 6 – Pressure fluctuation phase for OPA from the 2D calculation (at left) and the extraction at 80% blade height from the 3D calculation (at right), the line at Mach number equal to 1 is drawn in black.

regressive pressure waves which interact with the shock wave are induced by another source located at the first third of the chord. Despite these differences, around the traversing shock wave the phase pattern is similar in both cases on the pressure side.

On the suction side, in both cases regressive pressure waves reach the shock waves but with different propagation. At the upstream shock wave, regressive waves come from the downstream supersonic zone. In the 2D case pressure waves seem more straight and have fastest propagation than the 3D case. These pressure waves interact with the shock wave with a phase shift around 90° comparing 2D and 3D cases. Pressure waves in the last rear of the suction side also have a different propagation.In the 3D case the

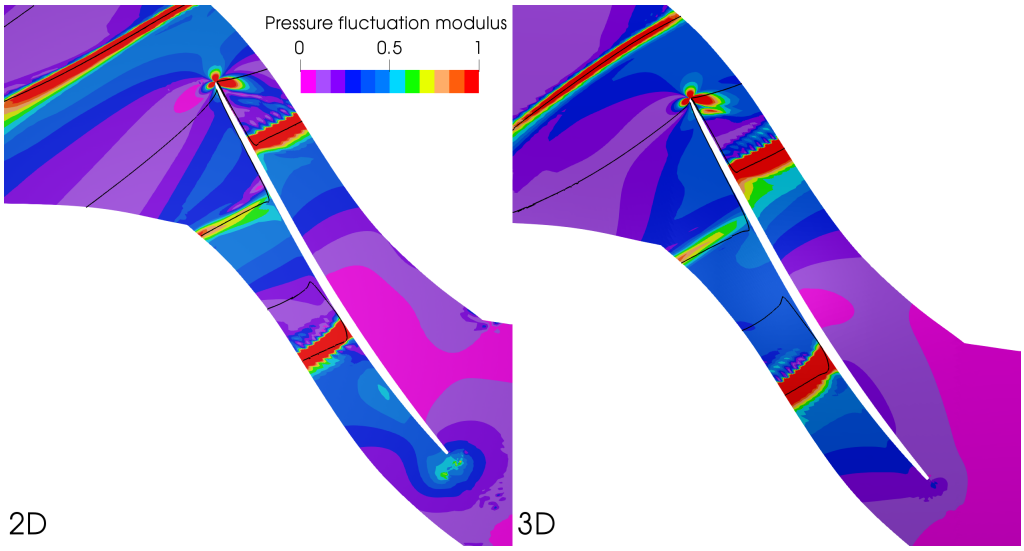

FIGURE 7 – Normalised pressure fluctuation modulus for OPB from the 2D calculation (at left) and the extraction at 80% blade height from the 3D calculation (at right), the line at Mach number equal to 1 is drawn in black.

pressure waves don't propagate (the phase is almost constant) in comparison to the 2D case. Again at the shock wave (downstream one this time) a phase shift between the two solutions around 120° is existing. The difference in terms of timing, or phase, in particular for the interaction with shock waves on the suction side seems the only explanation to the huge difference of work exchange between 2D and 3D cases. The question remains to know what can explain the differences of pressure wave propagation mechanism.

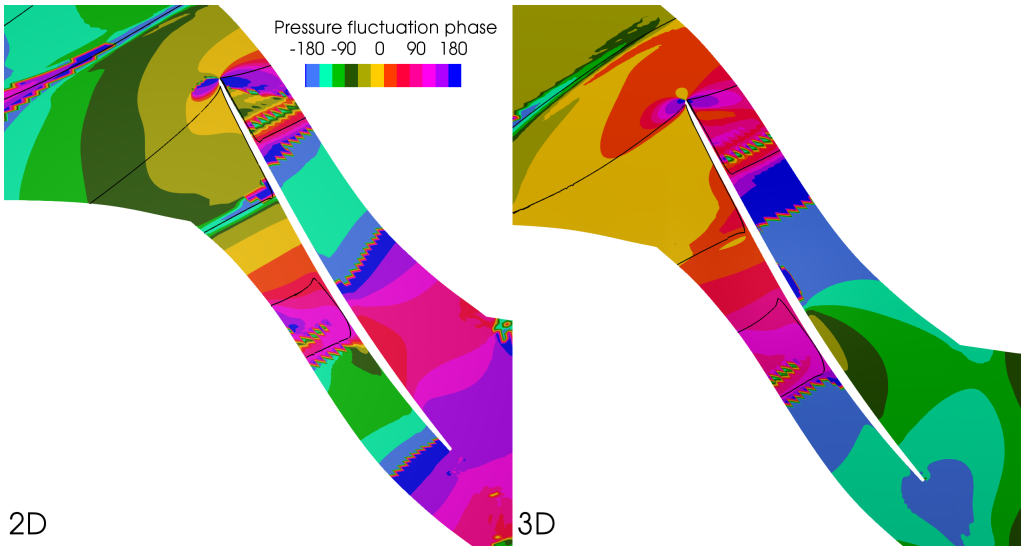

FIGURE 8 – Pressure fluctuation phase for OPB from the 2D calculation (at left) and the extraction at 80% blade height from the 3D calculation (at right), the line at Mach number equal to 1 is drawn in black.

4.3 Pressure waves propagation mechanism

The previous phase and modulus analysis is based on an abstract view of the pressure fluctuation. To go deeper in the understanding of the pressure wave propagation mechanism, the instantaneous aerodynamics fields have been animated during a complete vibration period for the 3D case. Pressure waves propagation and shock waves motion have been analysed on the 3D blade skin for both OP. The observed main mechanisms are summarised in fig. 9.

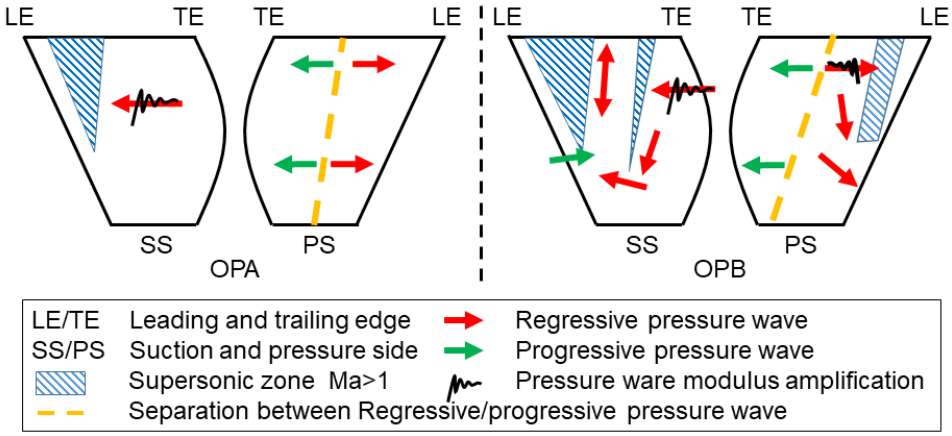

FIGURE 9 – Pressure wave propagation sketches for OPA (at left) and OPB (at right)

For OPA, the pressure waves propagate mostly in axial direction. On the suction side, regressive pressure waves interact with the shock wave and are amplified. In this case, 2D prediction can capture the main mechanism and prediction is not too far. The situation is completely different for OPB. On both sides, regressive pressure waves propogate to the downstream shock wave and are amplified. But in this case the shock wave chocks the interblade channel, therefore these pressure waves are blocked. But in 3D, the pressure waves can escape radially as shown in fig. 9. This mechanism cannot be reproduced by a 2D calculation. Additionally on the suction side, the deviated regressive pressure waves propagate radially up to the bottom of the supersonic zone. There regressive pressure waves can start again to propagate axially. So these pressure waves can now interact with the upstream shock waves and participate in its motion. This circumvention of the choked area and interaction with the upstream shock wave is, of course, impossible in a 2D calculation. An interesting fact, as can be noticed on the phase and modulus fields, is that this mechanism does not induce more intense pressure fluctuations but it has a strong influence on the waves propagation. In particular, the timing of the interaction between the regressive pressure waves and the upstream shock wave is impacted by the pressure waves emitted near the trailing edge. Near the hub, regressive pressure waves emitted from the trailing edge in the shroud region can propagate axially and modify the upstream shock wave motion. This effect induces a different timing over the complete blade height.

5 Conclusion

A high pressure axial compressor is analysed using linearised RANS simulations for two operating points at different rotational speeds. The first torsion mechanical mode has been imposed in both cases and the article focus on flutter onset. The flutter triggering prediction and the amount of work exchanged

between the fluid and the blade have been estimated with 3D calculation or from a 2D blade to blade cut at 80% height.

For the first operating point (OPA), the steady flow presents a large supersonic zone on the suction side near the leading edge, extending from the half of the blade height up to the shroud. 2D and 3D results show a good agreement in terms of work exchange and pressure fluctuations. The pressure waves tend to propagate axially and mechanisms can be captured by a 2D simulation. In this case a well-selected blade to blade cut can permit a good flutter triggering estimation.

For the second operating condition (OPB), the steady flow presents two large supersonic zones. The downstream shock wave chokes the interblade channel for a large part of the blade height. Even if the flutter triggering prediction is similar between 2D and 3D results (both cases have positive work exchange) the amount of work differs by one order of magnitude. In this case, the 3D motion of the regressive pressure waves allow a circumvention of the shock wave and the interaction with the upstream shock wave. This mechanism induces a different timing in the interaction with the shock wave and huge difference in the work exchange. The 2D calculation cannot predict this radial motion adequately and the flutter prediction is strongly impacted.

This work has to be completed with a larger number of test cases, to determine the different flow conditions where pressure wave radial propagation is important and requires a 3D calculation. According to the presented test cases, if a steady flow pattern presents multiple supersonic zones with a shock wave choking the interblade channel, a 3D calculation is recommended for the flutter triggering prediction.

Références

[1] M. Vahdati and N. Cumpsty Aeroelastic Instability in Transonic Fans *J. Eng. Gas Turbines Power 138(2), 022604*, 2015.

[2] P. Duquesne, B. Mahieux, S. Aubert, and P. Ferrand. Sensitivity of the aerodynamics damping coefficient prediction to the turbulence modelling conjugated with the vibration mode shape *13th European Conference on Turbomachinery Fluid dynamics and Thermodynamics,Lausanne, CH.*, 2019.

[3] O.C. Zienkiewicz and R.C. Taylor. Numerical Analysis of Fan Transonic Stall Flutter *ASME Turbo Expo 2014 : Turbine Technical Conference and Exposition, Dusseldorf, DE.*, 2014.

[4] Q. Rendu, L. Salles and M. Vahdati. Radial decomposition of blade vibration to identify stall flutter source in a transonic fan *15th International Symposium on Unsteady Aerodynamics, Aeroacoustics and Aeroelasticity of Turbomachines, Oxford, UK.*, 2018.

[5] A. Jameson, W. Schmidt and E. Turkel. Numerical solution of the Euler equations by finite volume methods using Runge Kutta time stepping schemes *14th Fluid and Plasma Dynamics Conference, American Institute of Aeronautics and Astronautics*, 1981.

[6] J. Kok. Improvements of two equations turbulence models in multi-block flow solvers : Freestream dependency and transition *Rapport technique, AVTAC/TR/NLR/JCK990520*, 1999

[7] M. Philit, P. Ferrand, S. Labit, J.-C. Chassaing, S. Aubert and T. Fransson. Derivated turbulence model to predict harmonic loads in transonic separated flows over a bump *28th International Congress of Aeronautical Sciences,Brisbane, AU.*, 2012.

[8] Q. Rendu, M. Philit, S. Labit, J.-C. Chassaing, Y. Rozenberg, S. Aubert and P. Ferrand. Time-linearized and harmonic balance Navier-Stokes computations of a transonic flow over an oscillating bump. *14th International Symposium on Unsteady Aerodynamics, Aeroacoustics and Aeroelasticity of Turbomachines, Stockholm, SE.*, 2015.

[9] J. Verdon. *Linearized unsteady aerodynamic theory*, AGARD Manuel on Aeroelasticity in Axial-Flow Turbomachines., 1989., Vol. **I**, 1987.